Phase diagram of hydrogen adsorbed on Ni(111)

Kiyoshi Nagai, Yuichi Ohno, and Takashi Nakamura
Research Institute for Catalysis, Hokkaido University, Sapporo 060, Japan
(Received 31 January 1984; revised manuscript received 30 April 1984)

The phase diagram for the H/Ni(111) system is calculated by treating a lattice gas on a honeycomb lattice through the position-space renormalization-group theory with prefacing transformation. The following interparticle interactions are considered: (A) nearest-neighbor exclusion, second-neighbor repulsion, and third-neighbor attraction, which was previously proposed by Domany *et al.*; (B) nearest-neighbor exclusion, second- and third-neighbor repulsions, and further-neighbor interactions up to the sixth-neighbor one. When the interaction parameters involved are suitably adjusted, both the interactions (A) and (B) lead to the phase diagrams in good agreement with the experimental one by Christmann *et al.* The change of the isosteric heat of hydrogen adsorption with the adsorbed amount is also calculated. The result obtained from interaction (B) is consistent with experiment, whereas that from interaction (A) is not.

I. INTRODUCTION

Varieties of long-period superstructures of adsorbates on metal surfaces have been reported.[1] Among them the H/Ni(111) system is a typical example; its phase diagram for the order-disorder transition has been obtained by Behm and Christmann and co-workers[2,3] from the temperature variation of the low-energy electron-diffraction (LEED) half-order spot intensity. The diagram shows a clear phase boundary but it is not symmetric about $\theta=0.5$, contrary to the expectation from the hole-particle symmetry on the triangular lattice, where θ is the ratio of the number of adsorbed particles to that of surface Ni atoms.

Afterwards, Domany, Schick, and Walker[4] (DSW) considered that this ordered phase is a (2×2) superstructure on a honeycomb lattice, and the phase diagram should therefore be symmetric about $n=0.5$, rather than about $\theta=0.5$, where n is the density defined as the ratio of the number of adsorbed particles to that of adsorption sites; i.e., $n=\theta/2$. Further, they obtained a phase diagram for a lattice gas (LG) on the honeycomb lattice through a renormalization-group (RG) calculation, in which infinite first-nearest-neighbor (1NN) and finite second-nearest-neighbor (2NN) repulsions are assumed. The phase diagram so obtained has a narrower width compared with that which is experimental [see Fig. 6(b)]. They predicted that this discrepancy is possibly solved by introducing an attractive third-nearest-neighbor (3NN) interaction and thus allowing for the appearance of a phase coexistence region on the lower density side.

Ostlund and Berker[5] (OB) devised a position-space RG method which can in principle include up to the 20NN interactions for a triangular LG. The main approximations in their method exist in a prefacing transformation which maps a LG Hamiltonian having first- and further-neighbor interactions onto a Hamiltonian with somewhat more complicated local degrees of freedom coupled by 1NN interactions only. They analyzed the phase diagrams of (2×2) and $(\sqrt{3}\times\sqrt{3})$ structures on the triangular LG system.

In the present paper, an alternative explanation to the above discrepancy encountered by DSW is proposed, where the 3NN repulsion rather than DSW's 3NN attraction is assumed. On this basis, a position-space RG calculation similar to OB is carried out to result in an appearance of a $p(2\times2)$ ordered phase centered at $n=\frac{1}{8}$, in addition to the (2×2) one at $n=\frac{1}{4}$. The calculated temperature versus density phase diagram well resembles the experimental one, and the calculated isosteric heat of adsorption shows a trend which supports the present proposal.

II. HAMILTONIAN AND SYMMETRY

Adsorption of the hydrogren atoms on the Ni(111) surface is believed to take place at the threefold hollow sites provided by the first-layer Ni atoms.[6,7] These hollow sites constitute a honeycomb lattice. Since theories indicate the existence of the long-range interactions between chemisorbed particles on metal surfaces via conduction electrons in the substrate,[8] a LG model on the honeycomb lattice with up to the sixth-nearest-neighbor (6NN) pairwise interaction is treated in the present work. Note that the 6NN distance, about 5 Å, is merely twice the lattice constant of the Ni surface layer, 2.49 Å.

The reduced (divided by $-k_BT$) Hamiltonian of the LG model is given as

$$H_{\rm LG}=-\mathscr{H}_{\rm LG}/k_BT=\sum_{m=1}^{6}J_m\sum_{\langle i,j\rangle}^{[m]}n_in_j-\mu\sum_i n_i\ , \quad (1)$$

where $H_{\rm LG}$, J_m, and μ are the Hamiltonian, the mth NN interaction, and chemical potential, respectively, all being reduced quantities; $n_i=1$ (0) when site i is occupied (empty), the first sum ranges from the 1NN to the 6NN, and the second sum over the $(i$-$j)$ pairs of sites at the mth NN distance apart. The diameter of the hydrogen in the chemisorbed state presumably does not exceed about 1.5 Å;[3] thus the 1NN interaction (at 1.44 Å apart) is taken to be the infinite repulsion.

The main high-symmetry-ordered structures expected to occur within 6NN interactions are $p(2\times2)$, $(\sqrt{7/3}\times\sqrt{7/3})$, $(\sqrt{3}\times\sqrt{3})$, (2×2), and (1×1) (Fig. 1). They have eightfold, sevenfold, sixfold, fourfold, and twofold degeneracies of sublattices, and include only the 6NN, 5NN, 4NN, 3NN, and 2NN interactions, respectively. There would occur many ordered structures other than those listed here depending on the choice of the parameters J_m's. However, since the experimental phase diagram has been obtained at relatively high temperatures (150–300 K),[3] we concentrate on the phases having (2×2) translational symmetry, which are expected to be stable in the above high-temperature range. This point is discussed in Sec. V in connection with the determination of the parameters J_m.

Let us investigate the symmetry relations between structures which include at least (2×2) translations. Let G_0 denote the group of symmetry operations which leaves the honeycomb lattice invariant; that is the group of symmetry of the disordered state (gas) or state at full coverage $(n=1)$. Further, the symmetry group of $p(2\times2)$, (2×2), and (1×1) ordered structures are denoted by $G_{p(2\times2)}$, $G_{(2\times2)}$, and $G_{(1\times1)}$, respectively. Then the relations between these G's are

$$G_0 \supset \begin{Bmatrix} G_{(2\times2)} \\ G_{(1\times1)} \end{Bmatrix} \supset G_{p(2\times2)} , \tag{2}$$

where $G_{(2\times2)}$ and $G_{(1\times1)}$ have no inclusion relation. It is easily seen that the factor group $G_0/T_{(2\times2)}$ is homomorphic with the cubic point group O_h, where $T_{(2\times2)}$ is the (2×2) translation group. This O_h is also equal to the symmetry of the spins in the site-diluted corner-cubic anisotropy classical Heisenberg (dCH) Hamiltonian defined in Sec. III. As seen from Eq. (2), $G_{p(2\times2)}$ is a subgroup of $G_{(2\times2)}$. Therefore, according to the Landau theory,[4,9] the phase transition between $p(2\times2)$ and (2×2) can be continuous. Since these two ordered structures have the same translational symmetry and cannot be distinguished by the diffraction experiments such as LEED without measuring, e.g., the spot intensities, they connect smoothly and are expected to form a wide (2×2) translational symmetry phase, i.e., $p(2\times2)$ plus (2×2), which is the experimentally observed one [see Fig. 6(b)].

More precisely, the threefold adsorption sites on the H/Ni(111) surface are classified into two groups, according to whether or not there exists a second-layer Ni atom below the site in question. Thus the honeycomb lattice (whose space-group symmetry is $p6mm$) is divided into two interpenetrating triangular lattices (space group $p3m1$);[10,11] the $p(2\times2)$ phase reduces to the (2×2) and the situation is described by adding a staggered field acting upon A, B, C, and D superlattices shown in Fig. 1(a) to Eq. (1). However, according to the idea of the crossover effect, if this staggered field is sufficiently weak, the results obtained for the $p6mm$-symmetry lattice describe well the real behavior except in the extreme vicinity of the critical points.[11]

It is known that the order-disorder phase transition the $p(2\times2)$ phase undergoes belongs to the Ising universality class, and that of the (2×2) belongs to the four-state Potts-model class,[10] but either can be first order as described in Sec. V A. If the space-group symmetry of the substrate is $p6mm$, then the $p(2\times2)$ phase can appear and if it is continuous transition the critical exponent of the Ising universality class will be observed. The recent experimental results on the O/Ni(111) system by Roelofs and co-workers[12,13] seem to suggest that this is the case.[13]

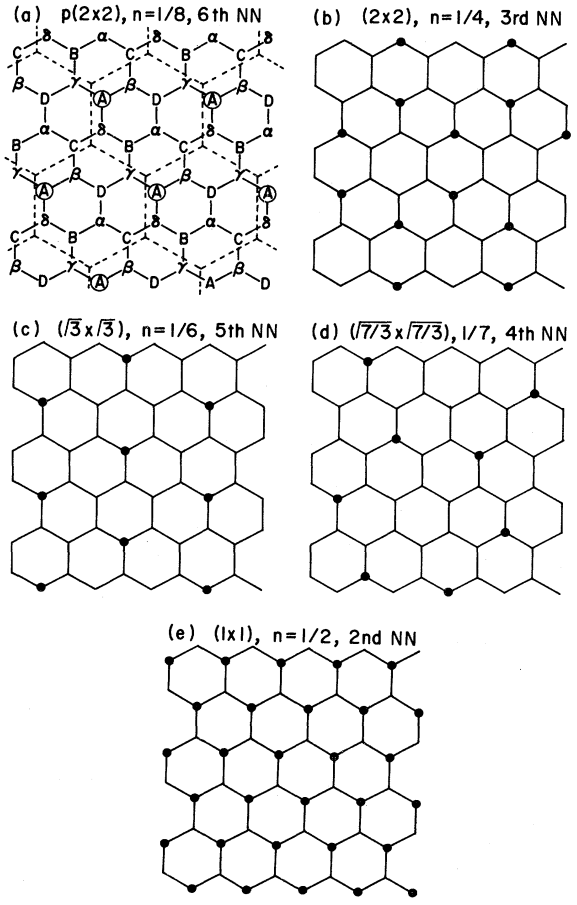

FIG. 1. Possible superstructures on the honeycomb lattice. (a) Unit cells are indicated with dashed lines and the eight $p(2\times2)$ sublattices are denoted by A, B, C, D, α, β, γ, and δ, respectively. (b)–(e) (2×2), $(\sqrt{3}\times\sqrt{3})$, $(\sqrt{7/3}\times\sqrt{7/3})$, and (1×1) occupations on the honeycomb lattice. The density and the interaction operative at the phase completion of each occupation are also shown.

III. METHOD

The calculational method used in this work follows the prescription given by OB (Ref. 5) and is briefly described in the following. The calculation starts with a LG Hamiltonian on a honeycomb lattice. Through a prefacing transformation, this LG Hamiltonian is converted into a dCH Hamiltonian[11,13] where spins on a triangular lattice are coupled by the 1NN interaction and each spin directs only to one of the eight corners of a cube. The prefacing transformation maps many further NN interactions in the LG Hamiltonian onto the more complicated local degrees of freedom coupled by the 1NN interaction in the dCH Hamiltonian. It also preserves the main symmetries of

the LG, i.e., $p(2\times2)$, (2×2), and (1×1). The dCH Hamiltonian is analyzed using a simple Migdal-Kadanoff—type RG method.

A. Prefacing transformation

Consider unit cells of (2×2) translational symmetry on the honeycomb LG, as shown with dashed lines in Fig. 1(a). The unit cell in the LG system becomes a supersite in the dCH system through the prefacing transformation as shown in Fig. 2, and the assembly of the supersites forms a triangular lattice. The reduced dCH Hamiltonian is expressed in spin representation as

$$H_{\rm dCH}=\sum_{\langle I,J\rangle} t_I t_J[\,K_1\vec{\rm S}_I\cdot\vec{\rm S}_J+K_2(\vec{\rm S}_I\cdot\vec{\rm S}_J)^2 +K_3(\vec{\rm S}_J\cdot\vec{\rm S}_J)^3+K_4]+\sum_I(K_5t_I+K_6)\,, \tag{3}$$

where I and J label supersites, and t_I and $\vec{\rm S}_I$ are the dilution operator ($t_I=0$ or 1) and spin variable with corner cubic anisotropy, $\vec{\rm S}_I=(\pm1,\pm1,\pm1)$, on supersite I, respectively. The spin variables appear in a inner-product form only, i.e., no field terms occur in Eq. (3). The first sum counts the 1NN pairs on the triangular lattice of supersites, and K_i's are reduced interaction parameters.

In the LG system, there are 2^8 configurations of particle occupation within a unit cell, but they reduce to 52 due to the 1NN exclusion, and the maximum number of occupation is 4. These 52 states in the LG unit cell are associated with nine states on a supersite in the dCH system as shown in Fig. 2. The nine states consist of a state for empty supersite ($t=0$), and eight states for occupied supersite and also with the spin pointing to one of the eight cubic corners [$t=1$ and $\vec{\rm S}=(\pm1,\pm1,\pm1)$], which are associated with the eight sublattices in the (2×2) translational symmetry.

The prefacing transformation, distributing 52 states into the nine states, obeys the equidistribution rule and is made precise with a projection operator. A configuration having no adatom in the unit cell is assigned to the empty supersite state, and that having one adatom is assigned to one of eight occupied supersite states with a corresponding spin direction. A configuration having two or more adatoms is equally shared by the eight occupied supersite states each with a corresponding spin direction. The projection operator has the value of 1/(number of recipient supersite states).

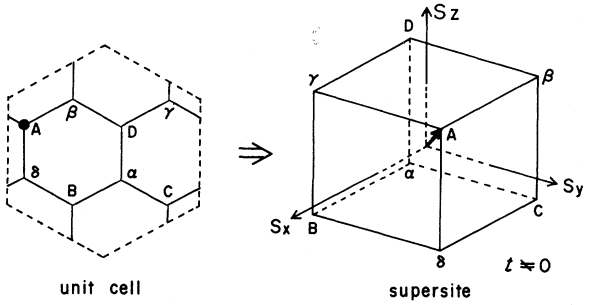

FIG. 2. Unit cell in LG and the supersite in dCH. An example of a case where the A site is occupied in the LG unit cell, which corresponds to $t=0$, and the spin at the dCH supersite directing to the A corner, is illustrated.

With the use of the projection operator, $P_I(t_I,\vec{\rm S}_I;\{n\}_I)$ for unit cell I, the prefacing transformation from the LG system to the dCH system is written as

$$\exp(H_{\rm dCH})=\mathop{\rm Tr}_{\{n\}}\prod_I P_I(t_I,\vec{\rm S}_I;\{n\}_I)\exp(H_{\rm LG})\,, \tag{4}$$

where I labels the unit cells in LG or supersites in the dCH, and $\{n\}_I$ is the assembly of occupation numbers, $\{n_A, n_B, n_C, n_D, n_\alpha, n_\beta, n_\gamma, n_\delta\}_I$, in unit cell I.

The prefacing transformation cannot be performed exactly. Therefore, the two-cell approximation is used which is the quasiperiodic boundary condition, realized by surrounding one unit cell by six replicas of the other,

$$\exp[6\tilde{H}_{\rm dCH}(I,J)]=\left\langle \mathop{\rm Tr}_{\{n\}_I,\{n\}_J} P_I P_J\exp\left[\sum_{\hat{r}} H_{\rm LG}(I,J)\right]\right\rangle_{\rm av}\,, \tag{5}$$

where the $\hat{r}$ sum runs over the six possible connections of the replicas, and $\langle\ \rangle_{\rm av}$ means the average over the 48 distinct ways of constructing unit cells on the honeycomb lattice. Each of these 48 ways corresponds to an element of the O_h group. Only in this averaging process the present calculation departs from the prescriptions by OB. The precise reasoning for this departure is discussed in the Appendix.

A dCH bond Hamiltonian denoted with a tilde is used in Eq. (5):

$$\tilde{H}_{\rm dCH}(I,J)=t_I t_J[\,K_1\vec{\rm S}_I\cdot\vec{\rm S}_J+K_2(\vec{\rm S}_I\cdot\vec{\rm S}_J)^2 +K_3(\vec{\rm S}_I\cdot\vec{\rm S}_J)^3+K_4] +(K_5/3)(t_I+t_J)+K_6/3\,, \tag{6}$$

in which the potential energy on a supersite are shared by the 1NN bonds pointing out of the supersite; the keypoint in the position-space RG treatment of keeping the ratio of the number of single-site energy to that of the pair-interaction energy on each site.[14] It should be noted that in the unit-cell pair Hamiltonian $H_{\rm LG}(I,J)$ given in Eq. (5), the intra-unit-cell interactions and chemical potential are grouped into the single-supersite energy, and the inter-unit-cell interaction into the pair-interaction energy.

B. Recursion equation

The dCH bond Hamiltonian on the triangular lattice is iterated through the simple Migdal-Kadanoff—type recursion equation. It is convenient to use the variables, which are the reduced pair energies E_i, between sites I and J, given by

$$\begin{bmatrix} E_1 \\ E_2 \\ E_3 \\ E_4 \\ E_5 \\ E_6 \end{bmatrix} = \begin{bmatrix} 3 & 9 & 27 & 1 & \frac{1}{3} & \frac{1}{3} \\ -1 & 1 & -1 & 1 & \frac{1}{3} & \frac{1}{3} \\ -3 & 9 & -27 & 1 & \frac{1}{3} & \frac{1}{3} \\ 1 & 1 & 1 & 1 & \frac{1}{3} & \frac{1}{3} \\ 0 & 0 & 0 & 0 & \frac{1}{6} & \frac{1}{3} \\ 0 & 0 & 0 & 0 & 0 & \frac{1}{3} \end{bmatrix} \begin{bmatrix} K_1 \\ K_2 \\ K_3 \\ K_4 \\ K_5 \\ K_6 \end{bmatrix} \begin{matrix} (\vec{S}_I \cdot \vec{S}_J = 3,\ t_I = t_J = 1) \\ (\vec{S}_I \cdot \vec{S}_J = -1,\ t_I = t_J = 1) \\ (\vec{S}_I \cdot \vec{S}_J = -3,\ t_I = t_J = 1) \\ (\vec{S}_I \cdot \vec{S}_J = 1,\ t_I = t_J = 1) \\ (t_I = 0, t_J = 1 \text{ or } t_I = 1, t_J = 0) \\ (t_I = t_J = 0) \end{matrix} , \tag{7}$$

where the states of supersites I and J are assigned by the values of the $\vec{S}_I \cdot \vec{S}_J$, and t_I, and t_J in the parentheses.

Then, using another group of parameters,[15]

$$\begin{aligned} X &= \exp(E_3 - E_1) , \\ Y &= \exp(E_2 - E_1) , \\ Z &= \exp(E_4 - E_1) , \\ S &= \exp(E_5 - E_1) , \\ T &= \exp(E_6 - E_1) , \end{aligned} \tag{8}$$

the recursion equation for the dCH model Eq. (5) can be expressed simply as

$$\begin{aligned} X' &= (2X^2 + 6Y^2Z^2 + S^4)/D , \\ Y' &= (2Y^2 + 2Y^4 + 2Z^4 + 2Z^2X^2 + S^4)/D , \\ Z' &= (2X^2Y^2 + 4Y^2Z^2 + 2Z^2 + S^4)/D , \\ S' &= (1 + X^2 + 3Y^2 + 3Z^2 + T^2)S^2/D , \\ T' &= (8S^4 + T^4)/D , \end{aligned} \tag{9}$$

where $D = 1 + X^4 + 3Y^4 + 3Z^4 + S^4$ and the transformed variables are denoted with a prime.

The range of variables X, Y, Z is $0 \le X, Y, Z \le 1$, showing that E_1, the reduced pair energy with spins parallel, is the largest of E_i's ($i = 1, \ldots, 4$), which in turn means a ferromagnetic regime (see also Table I). The region outside the ferromagnetic regime is an antiferromagnetic regime, which includes phases having translations disjoint with the (2×2), such as $(\sqrt{3} \times \sqrt{3})$ or $(\sqrt{7/3} \times \sqrt{7/3})$, etc. They are left out of consideration (see Sec. V). The regions for S, T variables are $0 \le S, T$. The limit $S = T = 0$ indicates that $E_1 \gg E_5, E_6$, and corresponds to the undiluted limit ($\langle t \rangle = 1$, where $\langle\ \rangle$ means thermodynamic average), where the spin order parameters discriminate the further division between solid and liquid. The limit $T \to \infty$ means $E_5, E_6 \gg E_1, \ldots, E_4$, and corresponds to the gas or diluted limit ($\langle t \rangle = 0$).

C. Physical quantities

The first derivatives of the free energy, such as density n or reduced internal energy E_{int}, are obtained as

$$\begin{aligned} n &= -\tfrac{1}{8} \sum_{a=1}^{6} \frac{\partial K_a}{\partial \mu} \phi_a(N/8) , \\ E_{\text{int}} &= \tfrac{1}{8} \sum_{a=1}^{6} \left[\sum_b \frac{\partial K_a}{\partial J_b} \right] \phi_a(N/8) , \end{aligned} \tag{10}$$

where

$$\phi_a(N/8) = \frac{1}{N/8} \frac{\partial \ln \Xi(N/8)}{\partial K_a} ,$$

and N is the number of the sites in the LG system and $\frac{1}{8}$ appears as the rate of coarse graining in the prefacing transformation. The ϕ_a is the derivative of the logarithm of the grand canonical partition function $\Xi(N/8)$ having $N/8$ supersites, and is calculated via the chain rule through iteration equation as

TABLE I. Five completely stable sink fixed points of dCH and their locations. The third and fourth columns provide the character of the phases, which are the domains of attraction of the fixed points. Interrelations between E_i's at the fixed points are listed in the fifth column, which also give the character of the phases. Ferro. indicates a ferromagnetic phase, PO Ferro. is the partially ordered ferromagnetic phase.

Sink points	Location (X, Y, Z, S, T)	Phases in LG	Phases in dCH	Relations between E_i's
L	(0,0,0,0,0)	$p(2\times2)$ solid	Ferro., $\langle t \rangle = 1$ 8P solid	$E_1 \gg E_2, \ldots, E_6$
4P	(1,0,0,0,0)	(2×2) solid	PO Ferro., $\langle t \rangle = 1$ 4P solid	$E_1 = E_3 \gg E_2, E_4, \ldots, E_6$
2P	(0,1,0,0,0)	(1×1) solid	PO Ferro., $\langle t \rangle = 1$ 2P solid	$E_1 = E_2 \gg E_3, \ldots, E_6$
Li	(1,1,1,0,0)	liquid	Spins disordered $\langle t \rangle = 1$, liquid	$E_1 = E_2 = E_3 = E_4 \gg E_5, E_6$
Gas	$(0,0,0,\infty,\infty)$	gas	$\langle t \rangle = 0$, gas	$E_5, E_6 \gg E_1, \ldots, E_4$

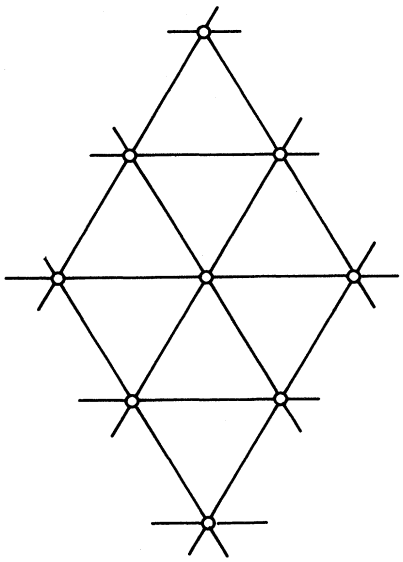

FIG. 3. Cluster consisting of nine supersites in dCH with a periodic boundary condition.

$$\phi_a(N/8)=\frac{1}{N/8}\frac{\partial \ln\Xi(N/8)}{\partial K_a}=\frac{1}{4}\sum_b \frac{\partial K_b'}{\partial K_a}\phi_b(N/8\times 4)$$
$$=\cdots=\frac{1}{4^n}\sum_{b_1}\cdots\sum_{b_n}\frac{\partial K_b'}{\partial K_a}\cdots\frac{\partial K_{b_n}^{(n)}}{\partial K_{b_{n-1}}^{(n-1)}}\times\frac{\partial \ln\Xi(N/8\times 4^n)}{\partial K_{b_n}^{(n)}}\,. \tag{11}$$

When the iteration of recursion converges, which is judged by the attainment of the stationary values in $(\partial K_a'/\partial K_b)$'s, the derivatives of the grand partition function $\partial \ln\Xi/\partial K_a$ is calculated for the cluster consisting of nine supersites with the periodic boundary condition shown in Fig. 3. Then the value of ϕ_a is obtained via Eq. (11).

IV. FIXED POINTS AND PHASE CORRESPONDENCE

There are a total of 45 fixed points in the five-dimensional interaction parameter space (X,Y,Z,S,T) of the dCH Hamiltonian. Among them, there are only five five-dimensional sink fixed points (or completely stable fixed points) which separate the five-dimensional space into five domains.[14] Each domain is assigned to one of the sink points into which the iteration starting from any point in the domain flows. The sink fixed points are listed in Table I. From the third and fourth columns, the relation between the phases in the LG and dCH systems can be found. The partially ordered phases of the 4P and 2P fixed points are distinguished by the equivalence of the two and four spin directions, respectively, as seen from the relations between E_i's given in the fifth column. The occurrence of the three phases, i.e., gas, liquid, and solid, follows from the introduction of the dilute variables in dCH.[14] The discussion of the remaining 40 fixed points and the global phase diagram of dCH will be given elsewhere.

V. RESULTS

Since our treatment includes interactions up to that which is 6NN, the values of five interaction parameters J_m $(m=2,\ldots,6)$ in Eq. (1) must be determined. (J_1 corresponds to the infinite repulsion mentioned in Sec. II.) There have been a few theoretical studies on the interaction between chemisorbed atoms on metallic surfaces.[8,16] According to these studies, the interaction seems to be much more complicated than that between rare-gas atoms physisorbed on solid surfaces;[5,14] for example, Muscat and Newns[16] have shown complicated variation of the interaction with interparticle distance. Although these theories are interesting, they are based on rather simplified models and the results do not seem to be conclusive. In our calculation, therefore, the relative magnitudes of J_m's are suitably varied so that the experimental phase diagram may be well reproduced.

Four sets of parameters to be considered in our work are listed in Table II. Note that our special concern here is how the sign of J_3 affects qualitatively the width of the (2×2) translational phases, as discussed at the ends of Secs. I and II. Set I is identical to that used by DSW,[4] and in set II the 3NN attractive interaction is added to set I according to DSW's suggestion.[4] Set III represents the explanation set forward in this work, and set IV is a variant of set III with attractive 3NN interaction.

A. Phase diagrams

The temperature versus chemical potential or density phase diagrams have been obtained for parameter set I and are shown in Fig. 4. In Fig. 4(b) the result by DSW,[4] who used the same parameter set, is also shown and com-

TABLE II. Parameter sets considered. Note that positive J_m implies an attractive interaction. The 1NN interaction is always taken to be infinite repulsion and J_2 to be finite repulsion. Attr. is the attractive interaction, and NNI is the nearest-neighbor interaction.

	Interaction parameter ratio				
Set	$J_3/\lvert J_2\rvert$	$J_4/\lvert J_2\rvert$	$J_5/\lvert J_2\rvert$	$J_6/\lvert J_2\rvert$	Remark
I	0	0	0	0	up to 2NNI
II	0.2	0	0	0	attr. 3NNI
III	−0.4	−0.8	−0.1	0.02	attr. 6NNI
IV	0.05	−0.8	−0.1	0.02	attr. 3NNI and 6NNI

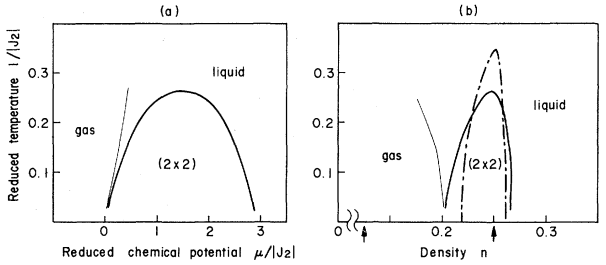

FIG. 4. Phase diagrams computed for parameter set I. (a) Temperature vs chemical potential. (b) Temperature vs density. Solid line: calculated continuous phase transitions; thin solid line: continuous change between two fluids, i.e., gas and liquid; dotted-dashed line: continuous transition obtained by DSW (Ref. 4). The arrows indicate the locations of the densities $n=\frac{1}{8}$ and $\frac{1}{4}$, at which the $p(2\times2)$ and (2×2) phases are complete.

pared with the present result. The maximum temperature of the (2×2) ordered phase obtained in our work is $1/|J_2|=0.26$, whereas that of DSW is 0.35. The width of the (2×2) phase of the former is a little larger than that of the latter. These differences seem to come from the approximations used in our work, i.e., the prefacing transformation and simple Migdal-Kadanoff procedure.

Figure 5 displays similar diagrams for set II. Introduction of the 3NN attraction produces a gas plus (2×2) coexistence region on the lower-density side. Incidentally, we have observed that as the 3NN interaction is made more attractive, the gas plus (2×2) coexistence region becomes wider. It is seen that Fig. 5(b) is in good agreement with the experimental phase diagram shown in Fig. 6(b), and thus corroborates DSW's prediction.

Now we are interested in the repulsive J_3 case. It is found that unless rather strong repulsive J_4 and J_5 are introduced, the phases $(\sqrt{3}\times\sqrt{3})$, $(\sqrt{7/3}\times\sqrt{7/3})$, etc. appear in the medium-density region of the phase diagram. These phases have not been found experimentally, at least in the experimental temperature range of 150–300 K. Therefore, the parameter search of set III has been carried out under the constraint that phases other than those with

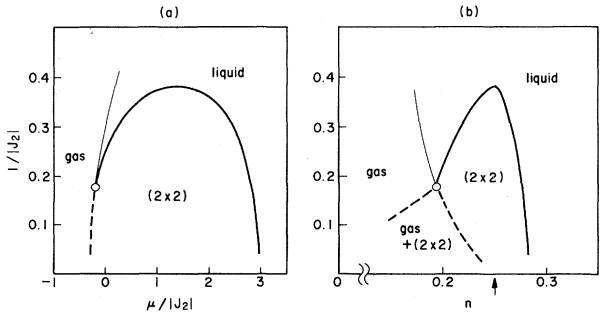

FIG. 5. Phase diagrams for the parameter set II. (a) Temperature vs chemical potential. (b) Temperature vs density. Solid line: calculated continuous phase transitions; thin solid line: continuous change between two fluids, i.e., gas and liquid; dashed lines: the first-order transition; open circles: multicritical points.

the (2×2) translational symmetry do not occur within the two-cell approximation described in Eq. (5). The result for set III so obtained is shown in Fig. 6. We observe that a $p(2\times2)$ phase appears and is in contact with the (2×2) phase, a portion of the boundary being a continuous transition. Therefore, the (2×2) translational symmetry region, $p(2\times2)+(2\times2)$, extends considerably wider than the case with the (2×2) phase only shown in Fig. 4 of set I. It has been found that if the weak 6NN attraction is converted to the repulsion with the same magnitude, the $p(2\times2)$ and the gas plus $p(2\times2)$ coexistence regions shrink to some extent although the qualitative features of the diagrams remain the same. In Fig. 7, the result for set IV (attractive 3NN case) is illustrated, where a gas plus (2×2) coexistence region appears as in Fig. 5.

From the exact result,[17] it is known that the q-state Potts model exhibits the first-order transition for $q>4$ and the continuous one for $q\leq4$. Furthermore, it is conjectured that the cubic N-vector model or O(N) model exhibits the first-order transition for $N>2$ and the continuous one for $N<2$.[18] The cubic model included in the dCH model is the $N=4$ case; hence the first-order transition is expected. On the other side, in the context of the diluted model, it is known that the phase transitions between an ordered solid and liquid is continuous and that between an ordered solid and gas is first order.[14] From the above information and the consideration of phase diagrams of the CH and dCH model planned to be published elsewhere, the following characterization of the phase boundaries in Fig. 6 can be given: The transition between liquid and (2×2) belongs to the four-state Potts criticality; both that between liquid and $p(2\times2)$, which does not occur in Fig. 6, and that between (2×2) and $p(2\times2)$ to the Ising criticality; that at the point where the gas, (2×2), and $p(2\times2)$ meet belongs to the cubic criticality, but it is a first-order transition, and all the other transitions appearing in Fig. 6 are of the first order.

It should be noted that the order-disorder transition of the $p(2\times2)$ phase [i.e., that between $p(2\times2)$ and the gas/solid] belongs to the Ising universality class. More precisely, that between $p(2\times2)$ and the liquid that does not occur in Fig. 6 is the Ising continuous transition, and that between $p(2\times2)$ and gas occurring in Fig. 6 is first order. Although the result, Fig. 6, indicates that the latter is the case, we cannot rule out the possibility of the former case of the continuous transition.

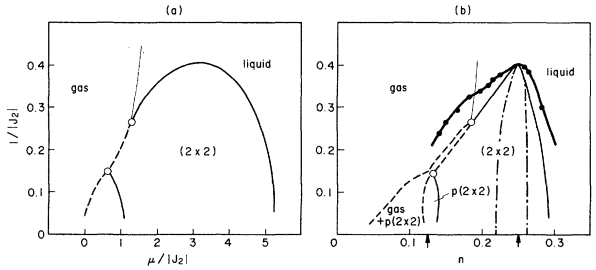

FIG. 6. Phase diagrams for parameter set III. (a) Temperature vs chemical potential. (b) Temperature vs density. Heavy line with closed circles: experimentally obtained boundary of (2×2) symmetry phase.

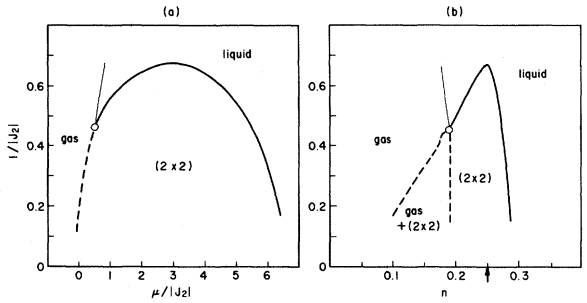

FIG. 7. Phase diagrams for parameter set IV. (a) Temperature vs chemical potential. (b) Temperature vs density.

B. Isosteric heat of adsorption

The isosteric heat of adsorption shown in Fig. 8 has been obtained for the H/Ni(111) system by Christmann *et al.*[19] They determined it from a series of isotherms ranging from 41 to 149 °C. Note that the temperature range is relatively high compared with $T_{\max}=270$ K in Fig. 6(b); in this range the adsorbed hydrogen is in the disordered phase.

The isosteric heat of adsorption $E_{\rm ad}$ is expressed according to thermodynamics as

$$E_{\rm ad}=h^g-2(\partial E_{\rm int}/\partial N)_{A,T}\ , \tag{12}$$

where h^g is the enthalpy per molecule of gaseous hydrogen which is taken to be an ideal gas, and A, N, and $E_{\rm int}$ are the area, number of hydrogen atoms, and the internal energy, respectively, of the adsorbed LG system. The derivative in Eq. (12) is calculated by numerical differentiation of $E_{\rm int}$ in Eq. (11). Only the derivative $-2(\partial E_{\rm int}/\partial N)_{A,T}$, is compared to the experimental $E_{\rm ad}$ in the following, because h^g is independent of n, and the relative variation of $E_{\rm ad}$ with the density n is of main interest here.

In Fig. 8, experimental data of $E_{\rm ad}$ versus work-function change $\Delta\phi$ are plotted.[19] With the use of the $\Delta\phi$ versus n data,[3] the points at which $n=\frac{1}{8}$ and $\frac{1}{4}$ are determined as shown with arrows in Fig. 8. Note that the location of the arrows should be taken approximate, since the $\Delta\phi$ versus n relation was obtained at $T=150$ K and the $E_{\rm ad}$ was determined from higher-temperature isotherms (see above).[3] The steplike decrease of $E_{\rm ad}$ in Fig. 8 with increasing density can be understood by considering the way in which stronger repulsions between hydrogen atoms at shorter distances become operative as the density increases.

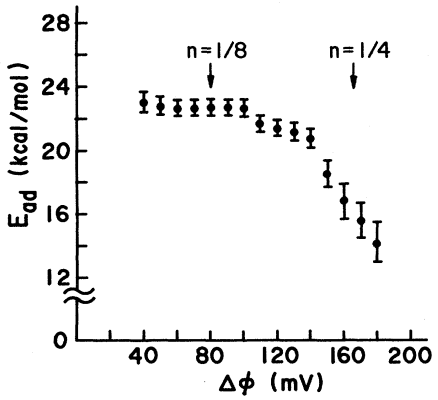

FIG. 8. Experimental isosteric heat of adsorption vs work-function change by Christmann *et al.* (Ref. 19) taken from a series of isotherms ranging from 41 to 149 °C. Arrows indicate the densities estimated from the $\Delta\phi$-vs-n data at 150 K.

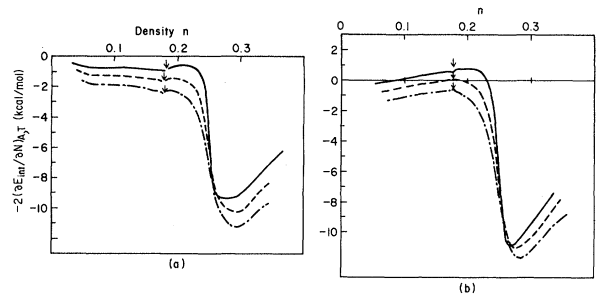

FIG. 9. $-2(\partial E_{\rm int}/\partial N)_{A,T}$ vs n diagrams. (a) That for parameter set I. (b) That for set II. The solid, dashed, and dotted-dashed lines represent the results at lower, medium, and higher temperatures, i.e., 41, 85, and 149 °C, respectively. The arrows indicate the point at which the recursion flow changes its sink point.

Figures 9 and 10 are $-2(\partial E_{\rm int}/\partial N)_{A,T}$ versus n diagrams computed by using parameter sets I–IV. The energy scales of the calculated $-2(\partial E_{\rm int}/\partial N)_{A,T}$ for each parameter set are determined by fitting the calculated $T_{\max}$ of the (2×2) phase to the experimental $T_{\max}=270$ K.[3,4] Experimental $E_{\rm ad}$ are obtained from the isotherms ranging from 41 to 149 °C, so that the three curves are calculated at lower (41 °C), medium (85 °C), and upper (149 °C) temperatures which are listed in each of the figures. From these figures, about a 8–10 kcal/mol decrease of $-2(\partial E_{\rm int}/\partial N)_{A,T}$ can be seen, in approximate agreement with experiment. We observe further that the introduction of the 3NN attraction in Figs. 9(b) and 10(b) leads to the increase of $-2(\partial E_{\rm int}/\partial N)_{A,T}$ with n in the region $n\lesssim 0.2$, which is contrary to the trend of the experimental $E_{\rm ad}$ in Fig. 8. Thus the possibility of the 3NN attraction suggested by DSW is excluded. Also, the introduction of further-neighbor interactions other than 3NN leads to the structure at around $n=0.1$ of the $-2(\partial E_{\rm int}/\partial N)_{A,T}$

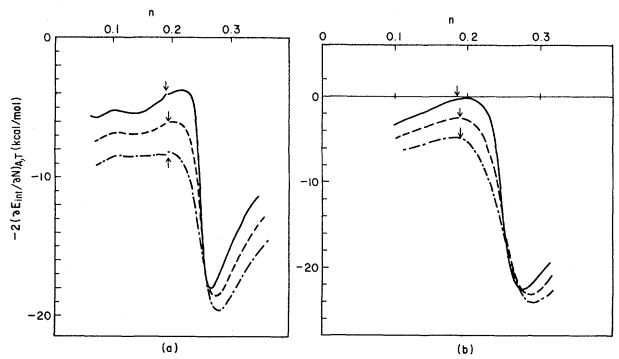

FIG. 10. $-2(\partial E_{\rm int}/\partial N)_{A,T}$ vs n diagrams. (a) That for parameter set III. (b) That for set IV.

curves in Fig. 10(a). We think that the structure may be related to the experimentally observed steplike drop of E_{ad} at around $\Delta\phi = 100$ mV in Fig. 8. The discontinuities near $n = 0.2$ marked with arrows in Figs. 9 and 10 are a computational artifact, i.e., they come from the fact that the sink point of the recursion iterations changes in going from gas to liquid at this point. It is possible that the entropy is counted differently in different phases in prefacing transformation, as discussed by Berker.[20]

VI. CONCLUDING REMARKS

In Sec. V, to interpret available experimental results for the H/Ni(111) system, two possibilities, (A) the J_3 attractive case and (B) the repulsive J_3 case, are examined in the same calculational framework. Both cases (A) and (B) reproduce well the main features of the experimental phase diagram. However, the calculated results in case (A) indicate that the isosteric heat of adsorption E_{ad} increases with the density n for $n \lesssim 0.2$, which is inconsistent with experiment, whereas case (B) is satisfactory in this respect. However, parameter set III determined as the result of optimization in case (B) exhibits somewhat unusual variation of the J_m's with distance. Especially, the relatively large ratio of J_4/J_3 is intriguing. More theoretical studies are certainly necessary to understand the interactions between chemsorbed atoms.

The effect of the second-layer Ni atoms is considered to be very small, but increasing its magnitude would give rise to a crossover of the critical behaviors from that of $p6mm$ space-group symmetry to that of $p3m1$ space-group symmetry. The crossover effect could be treated theoretically by adding the staggered field mentioned in Sec. II to the LG Hamiltonian, Eq. (1). For the system O/Ni(111), Roelofs *et al.*[12] have experimentally obtained the critical exponents, and shown that the critical behavior is probably that of $p6mm$ space-group symmetry. For the case of the H/Ni(111) system, the experimentally obtained critical exponent of the order-disorder transition of $p(2\times2)$ will be the Ising type for $p6mm$ space-group symmetry or the four-state Potts type for $p3m1$ space-group symmetry, if it is the continuous transition. Experimental establishment of the phase diagram in lower-temperature regions is highly desirable, although such experiments might be difficult. As seen from the comparison to DSW's result in Fig. 4 and as mentioned in Sec. V A, the present results are approximate, but qualitative features such as the phase connection or the characterization of phases should be reproduced correctly.

ACKNOWLEDGMENTS

The authors would like to thank Mr. M. Masuda and Dr. T. Matsushima for valuable discussions. All the numerical calculations have been performed on a HITAC M-200H computer at the Hokkaido University Computing Center. A grant support from the Ministry of Education, Science and Culture, Japan, is acknowledged with thanks.

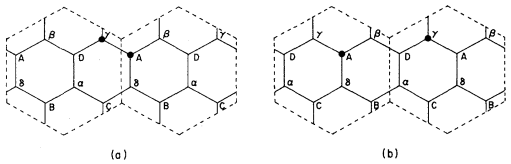

FIG. 11. Neighboring unit-cell pairs, an A site being occupied in one cell and a γ site in the other cell. (a) One of the 48 ways of unit-cell choices, where the A-γ pair is at the 1NN distance. (b) Another choice, where the A-γ pair is at the 4NN distance.

APPENDIX

The averaging over 48 ways of constructing unit cells on a honeycomb lattice is the crucial step in the prefacing transformation. Actually, in the projection step from unit cell to supersite, the symmetries in G_0 other than those in $G_{p(2\times2)}$ once vanish, and they are restored later through the averaging process. Also at the same time, various further-neighbor interactions in LG are approximated to yield the 1NN interaction in dCH.

The averaging used in this work is

$$\exp[6\tilde{H}_{\mathrm{dCH}}(I,J)] = \left\langle \operatorname*{Tr}_{\{n\}_I,\{n\}_J} P_I P_J \exp\left[\sum_{\hat{r}} H_{\mathrm{LG}}(I,J)\right]\right\rangle_{\mathrm{av}}, \tag{A1}$$

and the one by Ostlund and Berker is

$$6\tilde{H}_{\mathrm{dCH}}(I,J) = \left\langle \ln\left[\operatorname*{Tr}_{\{n\}_I,\{n\}_J} P_I P_J \exp\left[\sum_{\hat{r}} H_{\mathrm{LG}}(I,J)\right]\right]\right\rangle_{\mathrm{av}}, \tag{A2}$$

the former corresponding to the average on the level of partition function (or anneal-like average), and the latter on the level of physical quantity (quenchlike average).

Let us consider, for instance, two neighboring unit-cell pairs, each in the different unit-cell choices in the average $\langle\ \rangle_{\mathrm{av}}$, as shown in Figs. 11(a) and 11(b). In both cases, a cell has the A site occupied and the other cell has the γ site occupied, denoting one of the configurations in trace in Eqs. (A1) and (A2). They are either of the 1NN or the 4NN pairs. These 1NN and 4NN interactions must be averaged or approximated to give a single A-γ pair interaction of supersites. If Eq. (A1) is used, the resulting A-γ pair interaction stays finite; on the other hand, Eq. (A2) brings about infinite repulsion resulting from the 1NN infinite repulsion of LG. The average $\langle\ \rangle_{\mathrm{av}}$ is not only the symmetry-restoring process, but also the approximating process of the 1NN and 4NN interactions to the single interaction. Here we insist that the average must be taken by means of Eq. (A1), since the two interactions will be better averaged on the level of the partition function than the physical quantity.

It should be noted here that the degrees of freedom of the LG Hamiltonian is not identical to those of dCH. Precisely, the possibilities of multiple occupation on a unit cell in LG is suppressed on supersites in dCH.

[1]E. Bauer, in *Phase Transition in Surface Films,* edited by J. G. Dash and J. Ruvalds (Plenum, New York, 1980), p. 267.
[2]J. Behm, K. Christmann, and G. Ertl, Solid State Commun. **25**, 763 (1978).
[3]K. Christmann, R. J. Behm, G. Ertl, M. A. Van Hove, and W. H. Weinberg, J. Chem. Phys. **70**, 4168 (1979).
[4]E. Domany, M. Schick, and J. S. Walker, Solid State Commun. **30**, 331 (1979).
[5]S. Ostlund and A. N. Berker, Phys. Rev. B **21**, 5410 (1980).
[6]W. Ho, N. J. Dinardo, and E. W. Plummer, J. Vac. Sci. Technol. **17**, 134 (1980).
[7]G. Gasalone, M. G. Cattania, M. Simonetta, and M. Tescari, Chem. Phys. Lett. **61**, 36 (1979).
[8]T. B. Grimly and S. M. Walker, Surf. Sci. **14**, 395 (1969); K. H. Lau and W. Kohn, *ibid.* **75**, 69 (1978); V. Hartung, Z. Phys. **32**, 307 (1979).
[9]E. M. Lifschitz and M. Pitaevskii, *Statistical Physics,* 3rd ed. (Pergamon, New York, 1980), Part I, Chap. XIV.
[10]M. Schick, Prog. Surf. Sci. **11**, 245 (1981).
[11]M. Schick, Surf. Sci. **125**, 94 (1983).
[12]L. D. Roelofs, A. R. Kortan, T. L. Einstein, and R. L. Park, Phys. Rev. Lett. **46**, 1465 (1981); A. R. Kortan and R. L. Park, Phys. Rev. B **23**, 6340 (1981).
[13]M. Schick, Phys. Rev. Lett. **47**, 1347 (1981).
[14]A. N. Berker, S. Ostlund, and F. A. Putnum, Phys. Rev. B **17**, 3650 (1978).
[15]E. Domany and E. K. Riedel, Phys. Rev. B **19**, 5817 (1979).
[16]J. P. Muscat and D. M. Newns, Surf. Sci. **105**, 570 (1981); J. P. Muscat, *ibid.* **110**, 85 (1981).
[17]R. J. Baxter, J. Phys. C **6**, L445 (1973).
[18]B. Nienhuis, E. K. Riedel, and M. Schick, Phys. Rev. B **27**, 5625 (1983).
[19]K. Christmann, O. Schober, G. Ertl, and M. Neumann, J. Chem. Phys. **60**, 4528 (1974).
[20]A. N. Berker, in *Ordering in Two Dimensions,* edited by S. K. Sinha (Elsevier, New York, 1980), p. 15.